JOURNAL OF CATALYSIS 141, 171–190 (1993)

In Situ Electron Microscopy Studies of the Interaction of Iron, Cobalt, and Nickel with Molybdenum Disulfide Single Crystals in Hydrogen

B. H. UPTON, C. C. CHEN, N. M. RODRIGUEZ,[1] AND R. T. K. BAKER[1,2]

Department of Chemical Engineering, Auburn University, Auburn, Alabama 36849

Received May 4, 1992; revised November 24, 1992

Controlled atmosphere electron microscopy coupled with *in situ* electron diffraction has been used to examine the behavior of cobalt, nickel, and iron particles deposited on molybdenum disulfide when reacted in the presence of hydrogen. In addition to edge recession, a mode of attack also observed in the uncatalyzed reaction, it was evident in these systems that the metal particles were capable of facilitating the removal of sulfur atoms from the basal plane by a pitting action. Continuous observations of specimens undergoing reaction showed that metal particles exhibited several different morphologies and were constantly undergoing transformations. This phenomenon is explained in terms of the unusual bifunctional chemical character of the sulfide support which has a direct impact on the nature of the metal–support interaction. Electron diffraction analysis of specimens undergoing reaction in hydrogen indicated that a variety of compounds are possible including metal sulfides and intermetallics.

INTRODUCTION

Molybdenum disulfide, an important component of HDS catalysts, consists of a sandwich-like layered structure. Within the layers individual molybdenum atoms are surrounded by six sulfur atoms in a trigonal prismatic coordination, which forms the basis building block of the structure. Each sulfur atom in the extended lattice is strongly bound to three molybdenum atoms to form two-dimensional sheets. These triple-bonded sulfur atoms form the basal plane of the crystal (*1*). Because the sulfur atoms are so strongly bound in the basal plane they are chemically inert; however, the bonding between sulfur layers is relatively weak. When the molybdenum disulfide crystal is cleaved, the sulfur layers are easily detached from each other, leaving a monolayer of sulfur atoms on the basal plane (*2*). Various groups of workers have demonstrated that the edges of molybdenum disulfide are the most reactive regions of the structure toward both oxygen and hydrogen (*3–5*). Baker and co-workers (*5*) used controlled atmosphere electron microscopy (CAEM) to directly observe the reaction of molybdenum disulfide with oxygen and hydrogen and reported that oxygen attacked preferentially at the edge sites and point defects on the basal plane. Compared with oxidation, the reduction of molybdenum disulfide in hydrogen was relatively sluggish and attack occurred exclusively at edges, a finding which was consistent with the surface chemical studies of Farias and co-workers (*6*).

In many molybdenum disulfide-catalyzed reactions it is believed that the active sites are located at sulfur vacancies. Since the edge faces are composed of many such vacancies and molybdenum atoms with coordinated unsaturation, it is argued that these regions are more chemically active than the basal plane. This notion is supported by

[1] Present address: Materials Research Laboratory, The Pennsylvania State University, University Park, PA 16802.

[2] To whom correspondence should be addressed.

0021-9517/93 $5.00

high-resolution electron microscopy (*7*) and scanning Auger studies (*4*), which provide direct evidence that when cobalt/molybdenum disulfide specimens were treated at high temperature there was a tendency for the metal particles to migrate and accumulate at edge sites on the substrate.

A variety of surface science techniques have been applied to the study of the influence of deposited ferromagnetic metals on molybdenum disulfide single crystals (*8–10*). For the case of iron on molybdenum disulfide, studies were made of the system after heating up to 925°C under high-vacuum conditions (*8*). It was reported that at temperatures of about 525°C the agglomerated iron particles were capable of undergoing interaction with sulfur atoms in the basal plane of the substrate to create pits.

In the current investigation we have endeavored to look at these systems from a different perspective by using controlled atmosphere electron microscopy to directly observe the manner by which iron, cobalt, and nickel catalyze the reduction of molybdenum disulfide single crystals in the presence of hydrogen. In addition, these studies have been complemented by *in situ* electron diffraction experiments designed to determine the chemical state of the additives at various stages of the reaction. Macroscale thermogravimetric investigations were carried out in order to compare the microscopic behavior with that of bulk specimens.

EXPERIMENTAL

Studies of the dynamic behavior of individual metal particles on molybdenum disulfide were carried out in the controlled atmosphere electron microscope, the details of which can be found elsewhere (*11*). For these experiments transmission specimens (<50 nm thickness) of molybdenum disulfide were prepared by a standard cleaving procedure (*12*) from natural molybdenite originating from Froland, Norway. The particular transition metal under investigation was then deposited onto the sulfide by evaporation of spectrographically pure wire from a heated tungsten filament at a residual pressure of 10^{-6} Torr, in sufficient quantity to produce a metal coverage of about one monolayer. The specimen was then mounted in a gas reaction cell and inserted into the microscope.

The dynamics of the gas–solid reaction taking place at the specimen surface were displayed on a TV monitor and continuously recorded on video tape. Information from the tapes was measured by frame to frame analysis and the rates of motion of various events were evaluated as a function of temperature. From such data it was possible to determine the apparent activation energy for a given process.

In order to identify any spurious effects arising from the influence of the electron beam on either the gas or the solid specimen, blank experiments were performed on all systems. In this procedure the electron beam was turned off during the heating cycle and then the reacted specimen was examined on an intermittent basis at various stages of the reaction. Comparison of the appearance of this specimen with one under continuous observation enabled us to establish the form of any unusual behavior resulting from irradiation effects of the electron beam. In the current series of experiments no evidence for participation of the electron beam on the reactivity of the specimens was found.

The *in situ* electron diffraction experiments reported in this paper were carried out in a recently modified JEOL 200CX electron microscope (*13*). This instrumental approach not only provides higher resolution of the reactions between gases and solids (0.4 nm) but also allows for chemical analysis of the solid undergoing reaction from *in situ* electron diffraction. For these investigations somewhat heavier metal loadings, ~4 nm thickness, were introduced onto the molybdenum disulfide transmission specimens.

Electron diffraction patterns were taken at various stages of the reaction as specimens were heated in 0.2 Torr hydrogen. Care was taken to minimize the heating ef-

fects of the electron beam on the solid by operating at low intensity and by allowing the reaction to proceed to equilibrium with the beam turned off when not being used to obtain diffraction patterns. Analysis of the patterns was carried out by measuring the vector of the molybdenum disulfide substrate primary diffraction spots (d_{100} = 2.7324) and the radii of diffraction rings on the photographic negatives using a Rigaku powder camera film reader equipped with a vernier scale accurate to 0.05 mm. The sulfide primary diffraction spots were used as an internal standard to correct for variations in the camera length due to differences in the positions of the specimen or photographic plate. This procedure also serves to compensate for thermal expansion of the crystal lattice of the transition metal particle. Changes in d-spacing of the molybdenum disulfide substrate due to linear thermal expansion were calculated to be 0.41% at 400°C and 0.8% at 800°C. These values which were determined from the coefficient of thermal expansion of molybdenum disulfide, 10.7×10^{-6}/K (*14*), are taken into consideration in the analysis. The measured diffraction radii were then used to calculate the d-spacing of the crystallographic plane responsible for creating the diffraction rings and then compared to d-spacing values of possible reaction products as calculated from tabulated crystallographic data (*15–18*).

For the thermogravimetric studies of larger size samples of molybdenum disulfide, three different catalytic systems were investigated. Samples consisting of 5% cobalt, 5% nickel, and 5% iron, each supported on polycrystalline molybdenum disulfide, were prepared by the incipient wetness technique using the respective metal nitrate solutions. The polycrystalline molybdenum disulfide was obtained from Aldrich Chemicals and a BET nitrogen surface area measurement carried out on an Omnisorb 100CX unit gave a value of 6.3 m^2/g at −196°C. All samples were initially calcined in air at 200°C for 6 hr followed by reduction in 10% hydrogen/helium at 400°C for 12 hr and finally passivated in a 2% oxygen/argon mixture at room temperature. The passivated catalyst sample (~200 mg) was placed in a quartz dish suspended from a Cahn 2000 microbalance and initially given a short reduction treatment in 10% hydrogen/helium at 400°C prior to raising the temperature to reaction conditions. All reactions were performed in this mixture at atmospheric pressure and reaction rates were determined from initial weight-loss measurements.

The gases used in this work, hydrogen (99.999%), helium (99.99%), and argon (99.99%) were obtained from Alphagaz Co. and were used without further purification.

RESULTS

Controlled Atmosphere Electron Microscopy Studies

When molybdenum disulfide specimens containing a monolayer of iron, cobalt, or nickel were heated in hydrogen, the behavioral patterns of the three systems were very similar, differing only in the temperatures at which various events occurred. Therefore, for the sake of brevity a general description will be given, highlighting the reaction features and the corresponding temperatures for each system.

Prior to reaction in 1.0 Torr hydrogen, the profile of the edge and step regions of the molybdenum disulfide was relatively smooth and the basal planes were devoid of any major distinguishing characteristics. The first changes in the appearance of specimens were observed at temperatures over the range 200 to 250°C, when the edges tended to become corrugated in outline and this behavior was accompanied by the nucleation of small particles at these sites.

As the temperature was progressively raised these particles were seen to undergo a wetting and spreading action to form a thin film along the edge regions. An example of this type of behavior is shown for the Co/MoS_2 system in the sequence of photographs taken from the TV monitor, Figs. 1A–1D. Such an event was observed for

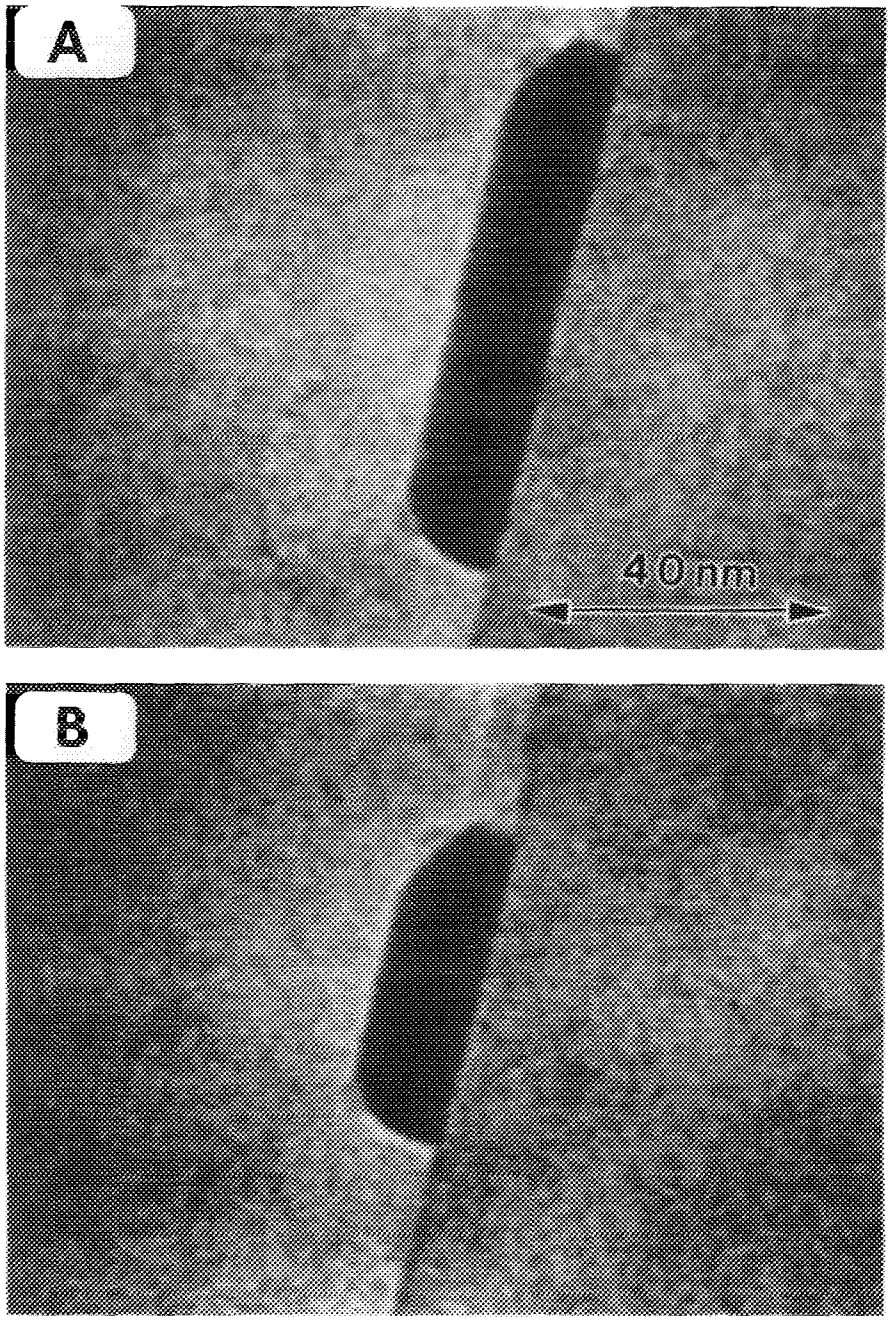

FIG. 1. Sequence showing the progressive spreading action of a cobalt particle on the edge of a molybdenum disulfide single crystal substrate in the presence of 1 Torr hydrogen at 475°C. The time between each frame is approximately 60 sec.

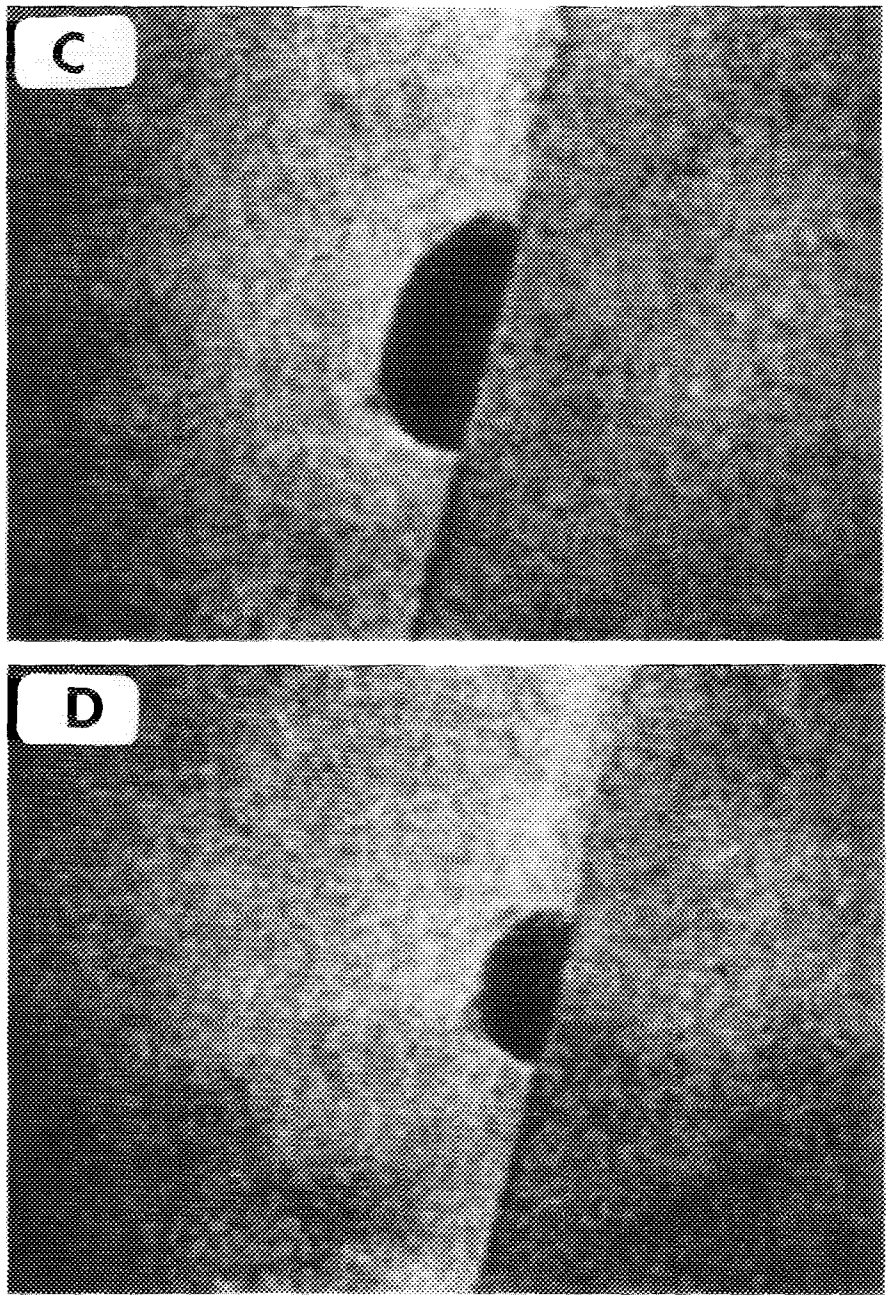

FIG. 1—*Continued*

iron particles at 365°C and for nickel and cobalt particles at 435°C and was the prelude to attack of the molybdenum disulfide. This action was manifested in the form of recession of the contaminated edges. In all cases, erosion of edges and steps by this mode of attack persisted up to between 535 and 550°C. At this stage there was a sudden change in the appearance of edges as needle-like structures began to form at these re-

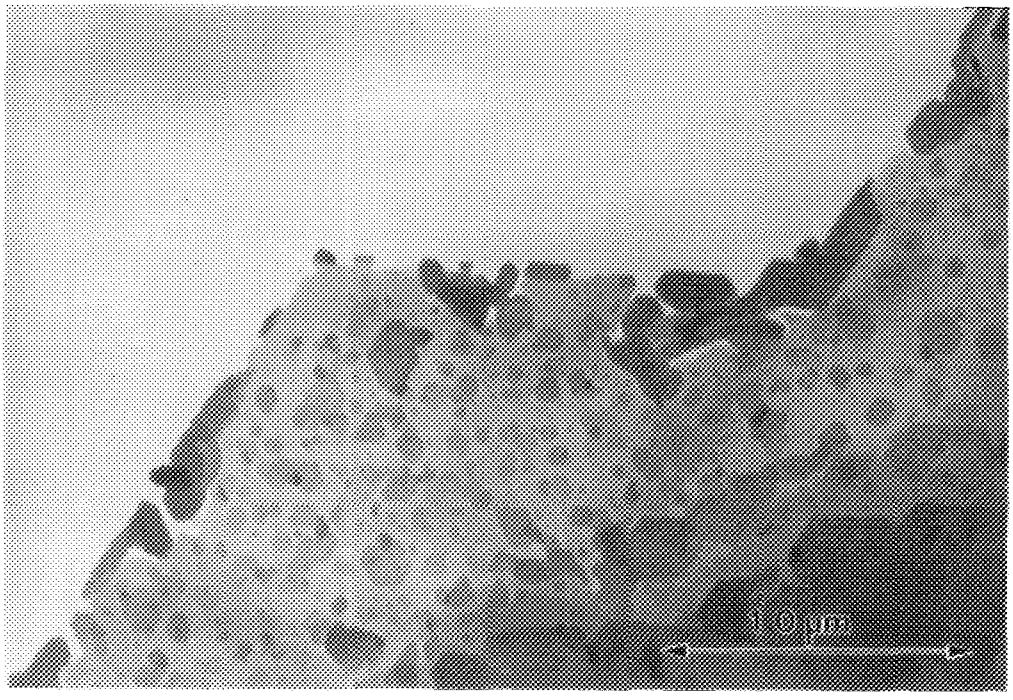

FIG. 2. Transmission electron micrograph of a cobalt/molybdenum disulfide specimen undergoing reaction in 0.2 Torr hydrogen at 600°C, showing the accumulation of crystallites at the edges of the substrate.

gions. Figure 2 is an electron micrograph taken during the reaction of a cobalt/molybdenum disulfide specimen with hydrogen at 600°C showing the accumulation of faceted structures formed at the edges of the substrate. From the micrograph one can clearly see the manner by which the formation of platelet structures is associated with the erosion of sulfide edge regions. Despite this change in the morphological appearance of edges removal of the sulfide continued; however, the reaction was limited to regions of contact between the substrate and the platelets, suggesting that the active catalytic entities were now incorporated in these structures. It was significant that these structures increased in size over a period of time and continuous observation of the process showed that such growth was associated with a concomitant loss of material from the molybdenum disulfide, suggesting that transport of material was taking place. Unfortunately, we are not in a position to determine the exact chemical identity of the platelet material since the electron diffraction data contain contributions from adjacent areas.

A survey of other areas of the specimens revealed that at temperatures between 550 and 600°C particles were also starting to collect on the basal planes, giving the surface a textured appearance. It was evident that there was a more visible concentration of catalyst particles at edge and step sites than on the basal plane regions. Initially particles which formed on the basal plane were globular in form, and on continued heating such particles increased in size and in some cases tended to acquire highly faceted outlines, with hexagonal shapes predominating. It was also apparent that the latter were responsible for catalyzing the creation of pits in the basal plane, a form of attack which was not observed when pristine samples of

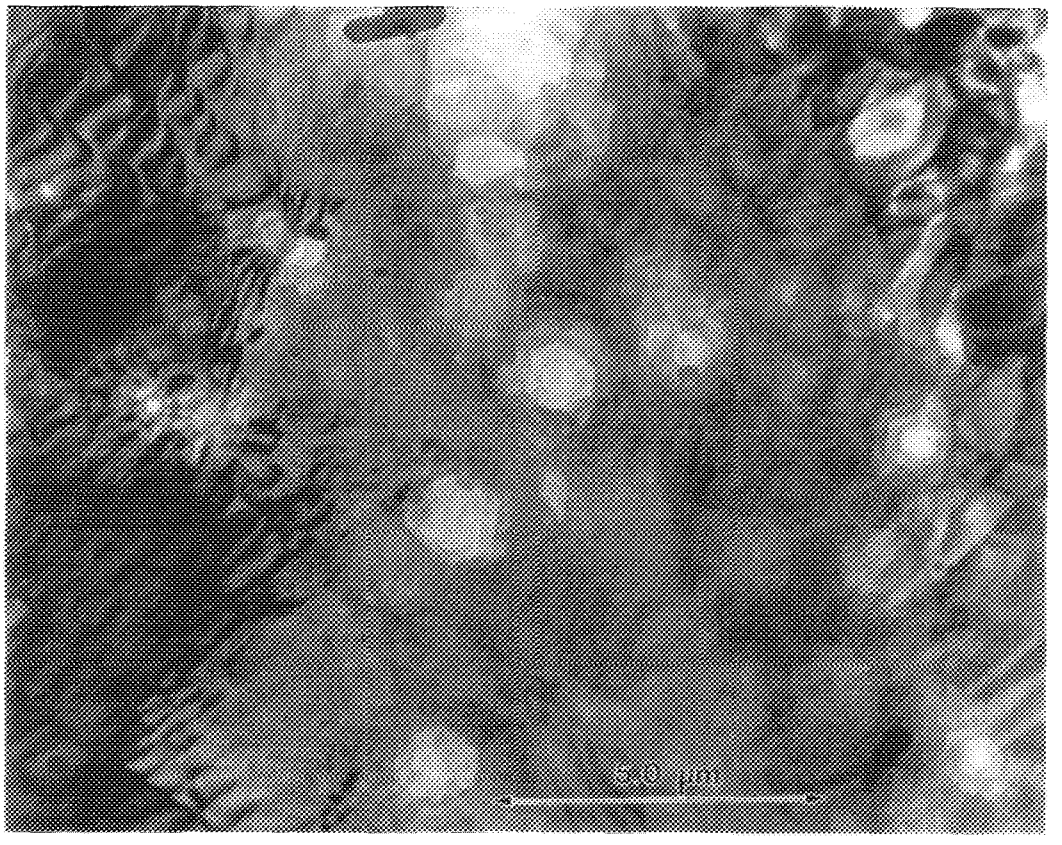

FIG. 3. Transmission electron micrograph of a cobalt/molybdenum disulfide specimen showing the formation of pits in the basal plane of the substrate after heating to 750°C in 2 Torr hydrogen.

molybdenum disulfide were reacted in hydrogen. As the reaction proceeded, the pits expanded laterally into well-defined hexagonal shapes and other concentric pits were produced in the lower layers of the substrate. A typical example of pits formed in the presence of added cobalt particles is presented in the electron micrograph of a specimen which had been cooled to room temperature after reaction at 750°C (Fig. 3). It was instructive to follow the behavior of metal particles associated with the pitting action. From a survey of many specimen areas some general features were evident.

(a) Particles located within the confines of the pit were faceted only at the points of contact with the sides of the pit and appeared to be quite globular at unattached regions.

(b) These particles constantly underwent a change in shape as the pit expanded, oscillating between a spread condition where the particle acquired the hexagonal shape of the pit and then after a short period of time reverting back to a more globular geometry. During this transformation particles occasionally ruptured into smaller fragments where a fraction of material maintained contact with the receding pit edges.

(c) In some cases where the expansion of a pit had developed to a considerable extent, the particles were no longer capable of maintaining their interaction with the edges and under such conditions would rapidly revert back to a globular form. It was significant

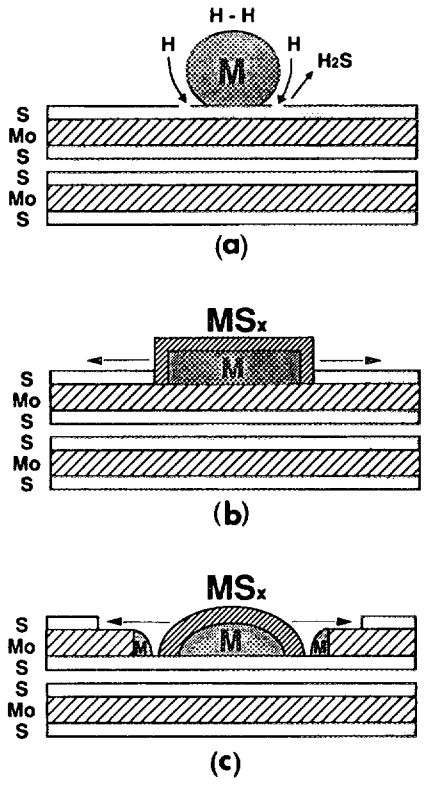

FIG. 4. Schematic representation of the changes in morphology of a metal particle during the creation of a pit in the basal plane. (a) The metal particle in contact with a sulfur layer in a nonwetting configuration initiating the reaction, (b) the sulfur covered metal particle exhibiting a strong interaction with a layer of molybdenum atoms in the substrate, and, (c) sulfur-covered metal particle once again in contact with a layer of sulfur atoms following a fragmentation step.

that when such an event took place there was no change in the rate of pit expansion suggesting that during this process a critical amount of the additive had remained attached to the pit walls. This behavior and the preceding steps are presented in the form of a schematic diagram (Fig. 4) and the underlying phenomena responsible for creating the changes in particle morphology are discussed later.

The rates of both edge recession and pit expansion showed a steady increase as the temperature was raised to 750°C. At temperatures above this level the reaction became so intense that disintegration of specimens frequently occurred with the result that most experiments were generally terminated at 800°C.

Detailed kinetic analysis from single frame projection of many recorded sequences showed that for each metal-based molybdenum disulfide system the rates of recession of edges were within experimental error, the same as those of pit expansion at any given temperature. The data obtained from such measurements are presented in the form of Arrhenius plots for the three systems in Fig. 5. Examination of these data indicates that of these three metals, iron is the most active catalyst for the reaction, with cobalt and nickel being very similar to each other. From the slopes of the lines it has been possible to derive the following apparent activation energies for the catalyzed reduction of molybdenum disulfide:

15.1 ± 2.0 kcal/mole for Ni,
16.9 ± 2.0 kcal/mole for Co,
19.3 ± 2.0 kcal/mole for Fe.

In Situ Electron Diffraction Studies

In this series of experiments the transition metal/molybdenum disulfide specimens were heated in the presence of 0.2 Torr hydrogen and electron diffraction patterns taken at selected temperatures during the reaction. In all cases attention was focused at the events occurring at the molybdenum disulfide edges, the areas of highest reactivity. As a consequence, information derived from the analysis of the electron diffraction patterns includes contributions from both the particles located on edges and those on the adjacent basal plane regions. In the specimen design utilized here the metal particles were exposed to two forms of sulfur. The primary source being that contained in the solid-phase, molybdenum disulfide, which is in direct contact with the metal particle. In addition the particles were exposed to gas-phase sulfur species resulting from H_2S, produced during reduction of the molybdenum disulfide substrate.

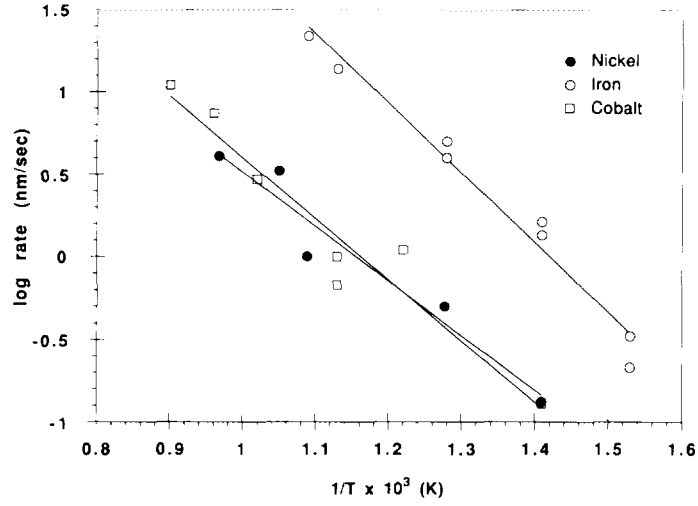

FIG. 5. Arrhenius plots for the metal-catalyzed reduction of molybdenum disulfide in 1.0 Torr hydrogen.

Co/MoS_2-H_2. The experimentally determined *d*-spacings of the various diffracting species are listed in Table 1 and a selection of patterns obtained at several temperatures are shown in Figs. 6A–6D. Inspection of the data shows that reduction of MoS_2 to Mo_2S_3 is possibly occurring at 500°C and interaction between cobalt and molybdenum to form alloys also appears to be a favorable process. It is interesting to find that the presence of metallic cobalt along with cobalt sulfide is indicated at all temperatures. Amorphous MoS_2 was included in all the electron diffraction analyses and could arise from fragmentation of the single crystal substrate or might correspond to mixed metal sulfides with equivalent *d*-spacings.

Ni/MoS_2-H_2. The *d*-spacings of the diffracting species for nickel on molybdenum disulfide as calculated from the data are presented in Table 2. The results clearly show a change in the chemical nature of the system as the temperature was progressively increased.

Fe/MoS_2-H_2. The Fe/MoS_2 system was the most complicated system studied as seen from the presence of a number of possible species indicated from these investigations (Table 3). In this system there was little evidence for the appearance of metallic iron until the temperature was increased to above 700°C. Inspection of the data shows that the alloys FeMo and Fe_2Mo along with both FeS and the mixed sulfide $FeMo_2S_4$ are formed during the catalyzed reduction of molybdenum disulfide.

In order to put these results into perspective with regard to the chemical nature of hydro-treating catalysts we have estimated the H_2S/H_2 ratio which is present in the gas-reaction cell at various stages of the catalytic reduction of MoS_2 by the three metals. The approach used for the calculations is given in the Appendix and the values obtained are presented in Table 4.

Thermogravimetric Studies

Thermogravimetric data of molybdenum disulfide in 10% hydrogen/helium both for uncatalyzed reactions and in the presence of each of the ferromagnetic metals are presented in graphic form in Fig. 7. The apparent activation energies of the uncatalyzed and catalyzed reactions were determined from the weight-loss measurements and were as follows:

TABLE I

Electron Diffraction Pattern Analysis of Co/MoS_2 as a Function of Temperature in 0.2 Torr H_2

Temperature (°C)	Calculated *d*-spacings (nm)	*d*-spacings (nm)						
		α-Co	β-Co	Co_2Mo_3	Co_3Mo	Co_9S_8	MoS_2[a]	Mo_2S_3
220	0.247						$0.250_{(0.12)}$	
	0.213	$0.217_{(100)}$	$0.205_{(100)}$					
	0.151	$0.148_{(012)}$						
500	0.248			$0.250_{(111)}$			$0.250_{(012)}$	
	0.215	$0.217_{(100)}$	$0.205_{(100)}$		$0.217_{(111)}$			$0.218_{(210)}$
	0.152	$0.148_{(012)}$		$0.152_{(023)}$	$0.151_{(202)}$		$0.153_{(112)}$	$0.151_{(121)}$
	0.129				$0.130_{(212)}$		$0.129_{(023)}$	$0.130_{(222)}$
	0.123	$0.125_{(110)}$	$0.125_{(220)}$		$0.123_{(310)}$		$0.125_{(024)}$	$0.125_{(320)}$
600	0.306			$0.308_{(300)}$			$0.308_{(004)}$	
	0.293			$0.292_{(310)}$				$0.297_{(200)}$
	0.250			$0.250_{(311)}$			$0.250_{(012)}$	
	0.233			$0.233_{(012)}$				$0.235_{(103)}$
	0.217	$0.217_{(100)}$			$0.217_{(111)}$			$0.218_{(210)}$
	0.205	$0.204_{(002)}$	$0.205_{(100)}$		$0.205_{(002)}$		$0.205_{(014)}$	$0.203_{(211)}$
	0.176	$0.177_{(200)}$	$0.177_{(200)}$					$0.176_{(014)}$
	0.153			$0.152_{(023)}$	$0.155_{(211)}$		$0.153_{(112)}$	$0.155_{(120)}$
	0.130				$0.130_{(212)}$		$0.130_{(023)}$	$0.130_{(222)}$
	0.125	$0.125_{(110)}$	$0.125_{(220)}$		$0.123_{(310)}$		$0.125_{(024)}$	$0.125_{(320)}$
655	0.500					$0.497_{(200)}$		
	0.307			$0.308_{(300)}$			$0.308_{(004)}$	
	0.292			$0.292_{(310)}$				
	0.251			$0.250_{(311)}$		$0.248_{(400)}$	$0.250_{(012)}$	
	0.234			$0.233_{(012)}$				$0.235_{(103)}$
	0.217	$0.217_{(100)}$			$0.217_{(111)}$			$0.218_{(210)}$
	0.203	$0.203_{(002)}$	$0.205_{(100)}$		$0.206_{(002)}$		$0.204_{(014)}$	$0.203_{(211)}$
	0.190	$0.192_{(101)}$		$0.190_{(302)}$				$0.190_{(113)}$
	0.177	$0.177_{(200)}$	$0.177_{(200)}$			$0.176_{(440)}$		$0.176_{(014)}$
	0.168				$0.168_{(210)}$			$0.169_{(310)}$
	0.153			$0.152_{(0.23)}$	$0.151_{(202)}$		$0.153_{(112)}$	$0.155_{(120)}$
	0.147	$0.148_{(012)}$			$0.148_{(300)}$		$0.147_{(113)}$	
	0.130				$0.130_{(212)}$		$0.130_{(023)}$	$0.130_{(222)}$
	0.125	$0.125_{(110)}$	$0.125_{(220)}$		$0.123_{(310)}$		$0.125_{(024)}$	$0.125_{(320)}$
705	0.502					$0.497_{(200)}$		
	0.360					$0.351_{(220)}$		
	0.305			$0.308_{(300)}$			$0.308_{(004)}$	
	0.289			$0.292_{(310)}$				
	0.249			$0.250_{(311)}$		$0.248_{(400)}$	$0.250_{(012)}$	
	0.231			$0.231_{(012)}$				
	0.217	$0.217_{(100)}$			$0.217_{(111)}$			$0.218_{(210)}$
	0.202	$0.203_{(002)}$	$0.205_{(100)}$		$0.206_{(002)}$		$0.204_{(014)}$	$0.203_{(211)}$
	0.190	$0.191_{(101)}$		$0.190_{(302)}$				$0.190_{(113)}$
	0.175	$0.177_{(200)}$	$0.177_{(200)}$			$0.176_{(440)}$		$0.176_{(014)}$
	0.167				$0.168_{(210)}$			$0.169_{(310)}$
	0.152			$0.152_{(023)}$	$0.151_{(202)}$		$0.153_{(112)}$	$0.151_{(121)}$
	0.145	$0.148_{(012)}$			$0.148_{(300)}$		$0.147_{(113)}$	
	0.137				$0.139_{(301)}$		$0.137_{(200)}$	$0.137_{(221)}$
	0.131				$0.131_{(212)}$		$0.130_{(023)}$	$0.130_{(222)}$
	0.124	$0.125_{(110)}$	$0.125_{(220)}$		$0.123_{(310)}$		$0.125_{(024)}$	$0.125_{(320)}$
	0.115	$0.115_{(013)}$						

TABLE I—*Continued*

Temperature (°C)	Calculated *d*-spacings (nm)	*d*-spacings (nm)						
		α-Co	β-Co	Co_2Mo_3	Co_3Mo	Co_9S_8	MoS_2[a]	Mo_2S_3
755	0.307			$0.308_{(300)}$			$0.308_{(004)}$	
	0.251			$0.250_{(311)}$		$0.248_{(400)}$	$0.250_{(012)}$	
	0.233			$0.231_{(012)}$				$0.235_{(103)}$
	0.218	$0.217_{(100)}$	$0.205_{(100)}$		$0.217_{(111)}$			$0.218_{(210)}$
	0.154			$0.152_{(023)}$	$0.155_{(211)}$		$0.153_{(112)}$	$0.155_{(120)}$
	0.132				$0.131_{(212)}$		$0.130_{(023)}$	$0.130_{(222)}$
	0.125	$0.125_{(110)}$	$0.125_{(220)}$		$0.123_{(310)}$		$0.125_{(024)}$	$0.125_{(320)}$

[a] The amorphous MoS_2 pattern may correspond to a Co–Mo–S phase.

23.9 ± 2.0 kcal/mole (uncatalyzed),
17.0 ± 2.0 kcal/mole for Co,
16.5 ± 2.0 kcal/mole for Ni,
21.1 ± 2.0 kcal/mole for Fe.

For each of the transition metals studied as catalysts, an increase in the rate of reaction was observed, although this effect diminished as the temperature was raised above 900°C. The iron catalyst was found to induce the highest reaction rates despite the finding that the activation energy was higher than that when either cobalt or nickel were introduced onto the sulfide.

DISCUSSION

The results of this study clearly demonstrate that iron-, cobalt-, and nickel-based catalysts exert a significant influence on the hydrogenation of molybdenum disulfide. Both micro- and macroscale experiments indicate that of the three metals, particles derived from iron are the most active catalyst for this reaction. Direct observation of the behavior of these systems in the controlled atmosphere electron microscope indicates that they exhibit many common characteristics in their catalytic action. It was evident that when particles of these metals came into contact with the molybdenum disulfide crystal edges they underwent a rapid wetting and spreading action, indicative of a strong interaction between the particle and the support medium. These findings are consistent with those reported in previous studies (*4*, *7*) which showed that in HDS catalysts cobalt was located at edge positions of the molybdenum disulfide structures. The maximum amount of metal additive that can be accommodated at such regions is obviously going to be a function of the available surface area of the sulfide crystals. With the type of specimens used in the current experiments, the accessible edge area is relatively low and consequently a large fraction of the deposited metal atoms tend to remain on the basal planes of the sulfide crystals.

An extremely important aspect to emerge from the present investigation was the finding that in addition to promoting attack at edge and steps sites of the crystal, the catalytic entities were also found to be capable of creating hexagonal-shaped pits in the basal plane regions. It is possible that pits are initiated when the catalyst particle encounters a surface defect, such as a vacancy or point defect at an emergent screw dislocation. The bifunctional chemical nature of the molybdenum disulfide is responsible for generating a rather unusual pattern of behavior with respect to transformations in the morphology of metal particles located on the basal plane of the support, which can be correlated with changes in the strength of the metal–support interaction. The series of proposed steps involved in the creation and development of pits are outlined in the schematic diagram shown in Figs. 4a–4c.

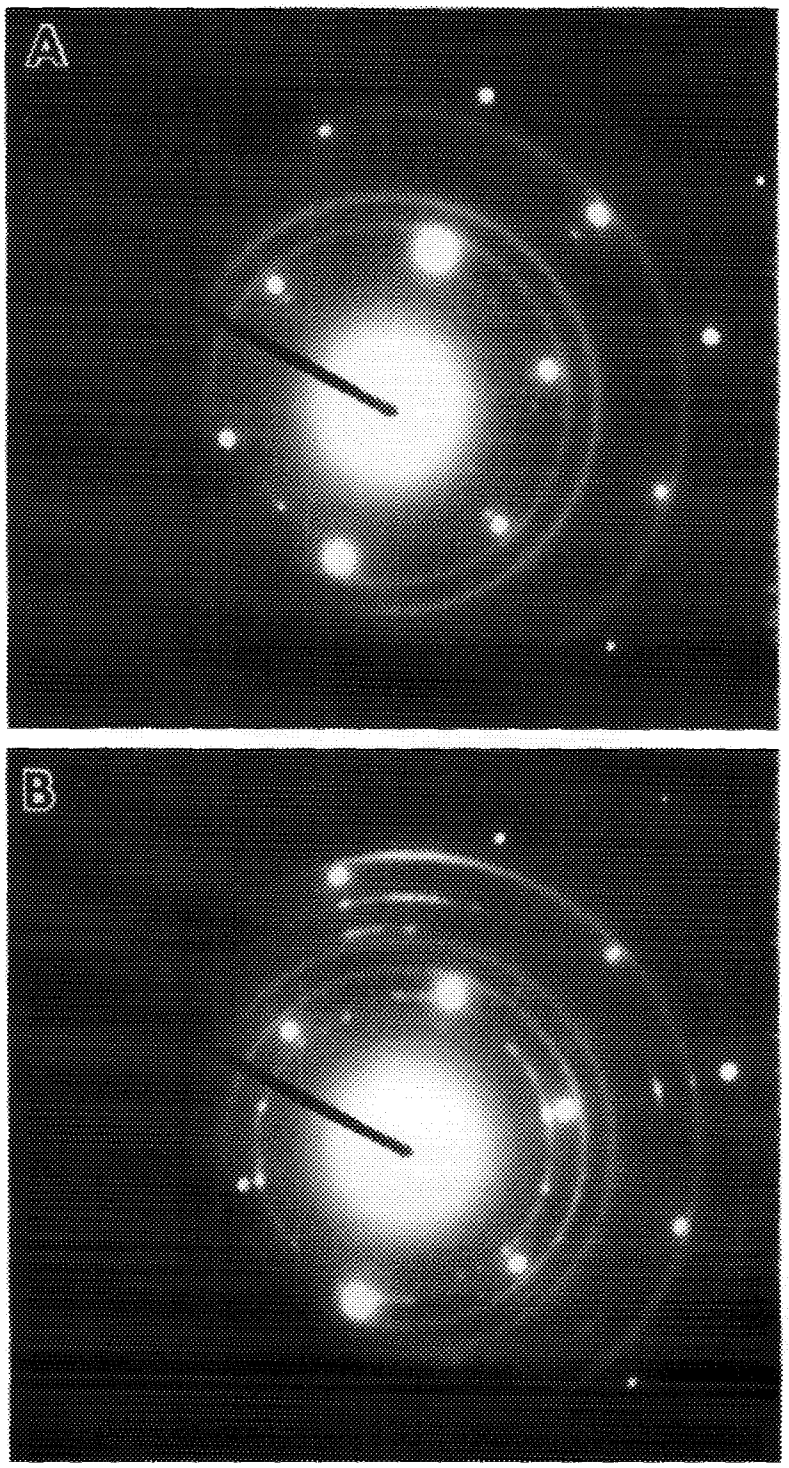

FIG. 6. Selected area electron diffraction patterns of cobalt/molybdenum disulfide specimens at various temperatures in 0.2 Torr hydrogen. (A) 500°C, (B) 635°C, (C) 705°C, and (D) 755°C.

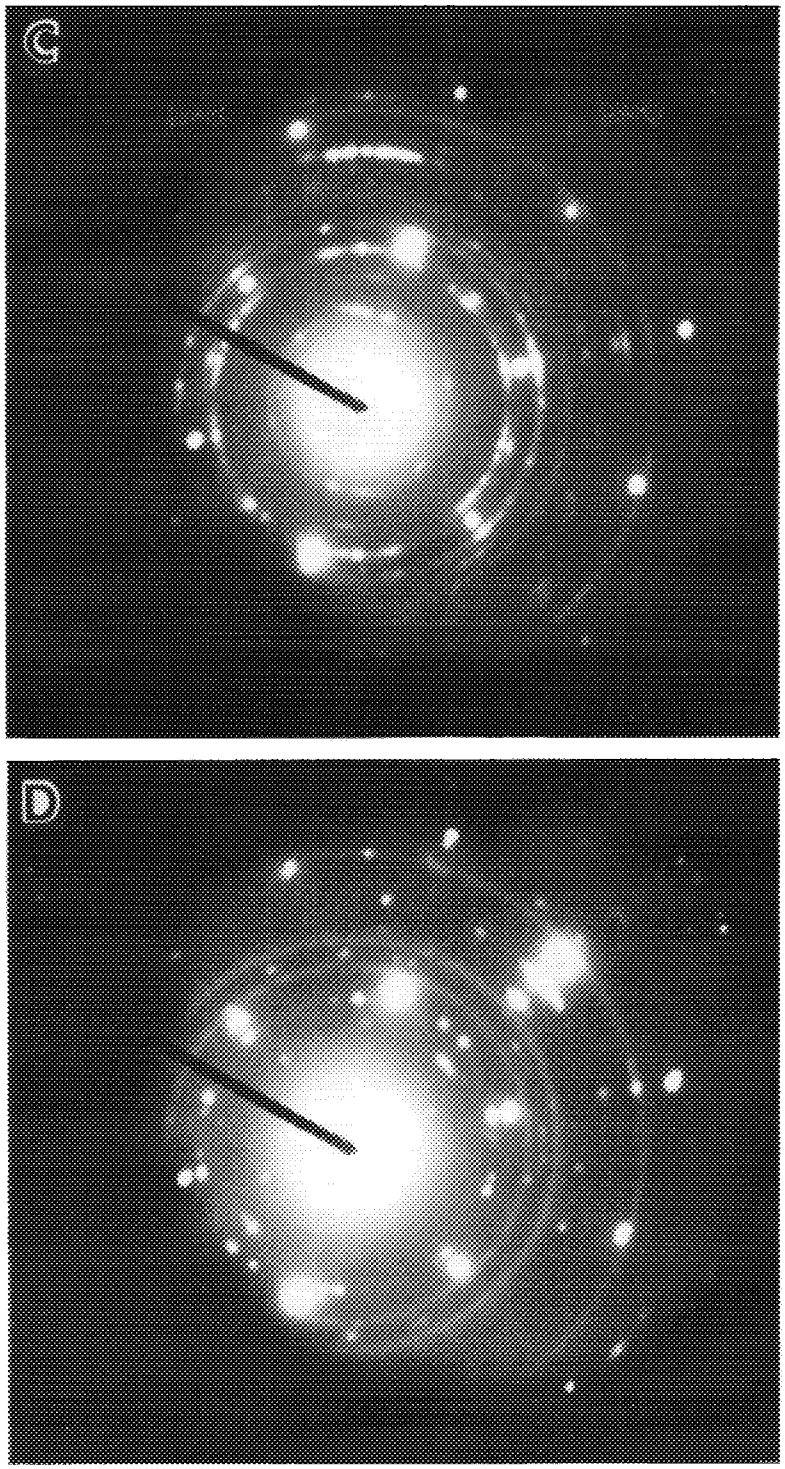

FIG. 6—*Continued*

TABLE 2

Electron Diffraction Pattern Analysis of Ni/MoS_2 as a Function of Temperature in 0.2 Torr H_2

Temperature (°C)	Calculated *d*-spacings (nm)	*d*-spacings (nm)						
		Ni	NiMo	Ni_4Mo	Ni_3S_2	NiS	MoS_2[a]	Mo_2S_3
210	0.211	$0.203_{(111)}$	$0.209_{(002)}$			—		
305	0.229							
	0.217		$0.220_{(100)}$					$0.218_{(210)}$
	0.203	$0.203_{(111)}$			$0.204_{(202)}$		$0.205_{(006)}$	$0.203_{(211)}$
	0.177	$0.176_{(200)}$		$0.178_{(002)}$	$0.178_{(004)}$			$0.176_{(014)}$
	0.157				$0.157_{(311)}$			
410	0.205	$0.203_{(111)}$			$0.204_{(202)}$		$0.205_{(006)}$	$0.203_{(211)}$
	0.178	$0.176_{(200)}$		$0.178_{(002)}$	$0.178_{(004)}$			$0.176_{(014)}$
510	0.244				$0.235_{(021)}$	$0.240_{(220)}$	$0.250_{(012)}$	
	0.210	$0.203_{(111)}$	$0.209_{(002)}$		$0.204_{(202)}$		$0.205_{(006)}$	
	0.148		$0.151_{(012)}$	$0.151_{(202)}$		$0.147_{(202)}$		
610	0.344							
	0.243					$0.240_{(220)}$	$0.250_{(012)}$	
	0.218		$0.220_{(100)}$					
	0.184					$0.186_{(131)}$	$0.183_{(015)}$	
	0.172	$0.176_{(200)}$			$0.183_{(113)}$	$0.174_{(401)}$		$0.176_{(014)}$
	0.154		$0.151_{(012)}$	$0.151_{(202)}$		$0.155_{(012)}$	$0.153_{(112)}$	$0.155_{(120)}$

[a] The amorphous MoS_2 pattern may correspond to a Ni–Mo–S phase.

In the early stages of the reaction, the metal particle is in contact with a surface consisting of sulfur atoms and in this state it is likely that a relatively weak metal–support interaction exists. In these circumstances the metal particle will tend to assume the energetically preferred configuration of a globule (Fig. 4a). As the reaction proceeds, expansion of the pit occurs via a process involving hydrogen dissociation on the metal particle surface followed by spillover to the adjacent sulfur layer in the support and ultimate removal of S-H groups as H_2S. As such atoms are progressively removed, the catalyst particle now encounters a layer of molybdenum atoms and a strong interaction is established, which results in the particle undergoing a spreading action (Fig. 4b). Under this condition the particle shape is dictated by that of the hexagonal-shaped pit. The appearance of such faceted particles enables one to detect the presence of monolayer pits, which could not be observed by conventional transmission electron microscopy since the difference in electron scattering density between the pit base and that of the surrounding unattacked support material is negligible.

In contrast, when the sulfur-covered particle once again comes into contact with a basal plane surface comprised of sulfur atoms, the metal–support interaction is weakened at these points of contact and there will be a tendency for the particle to revert back to a globular form. A fraction of the particle material, believed to be in the metallic state, will remain in contact with the molybdenum atoms at the reactive edges of the pit, where a strong interaction will be preserved. Under the influence of these opposing forces it is not surprising to find that the particle undergoes fragmentation (Fig. 4c). As the reaction proceeds, pits become deeper and the sequence will be repeated. This pattern of behavior would be

TABLE 3

Electron Diffraction Pattern Analysis of Fe/MoS_2 as a Function of Temperature in 0.2 Torr H_2

Temperature (°C)	Calculated *d*-spacings (nm)	*d*-spacings (nm)						
		Fe	FeMo	Fe_2Mo	FeS	$FeMo_2S_4$	MoS_2[a]	Mo_2S_3
225	0.302				$0.298_{(110)}$			
	0.258				$0.258_{(200)}$			
	0.213					$0.211_{(313)}$		
505	0.480				$0.473_{(101)}$	$0.468_{(111)}$		
	0.297				$0.298_{(110)}$	$0.296_{(004)}$		$0.297_{(200)}$
	0.254		$0.256_{(320)}$		$0.258_{(200)}$			
	0.210		$0.213_{(202)}$			$0.211_{(313)}$		
	0.161		$0.161_{(332)}$		$0.163_{(124)}$	$0.163_{(040)}$	$0.147_{(113)}$	
	0.148		$0.149_{(123)}$		$0.149_{(220)}$	$0.147_{(242)}$		
580	0.480				$0.473_{(101)}$	$0.468_{(111)}$		
	0.301				$0.298_{(110)}$	$0.296_{(004)}$		$0.297_{(200)}$
	0.255		$0.256_{(320)}$		$0.258_{(200)}$			
	0.173			$0.175_{(113)}$	$0.172_{(300)}$			$0.176_{(014)}$
	0.163		$0.163_{(440)}$	$0.161_{(023)}$	$0.163_{(14)}$	$0.163_{(040)}$		
	0.149		$0.149_{(123)}$		$0.149_{(220)}$	$0.147_{(242)}$		
665	0.549					$0.558_{(110)}$		
	0.480				$0.473_{(101)}$	$0.468_{(111)}$		
	0.407			$0.411_{(100)}$				
	0.322					$0.327_{(020)}$		
	0.297				$0.298_{(110)}$	$0.296_{(004)}$		$0.297_{(200)}$
	0.256		$0.256_{(320)}$		$0.258_{(200)}$			
	0.211		$0.213_{(202)}$	$0.205_{(200)}$		$0.211_{(313)}$		
	0.172			$0.175_{(113)}$	$0.172_{(300)}$			
	0.162		$0.163_{(124)}$	$0.161_{(023)}$	$0.163_{(124)}$	$0.163_{(040)}$	$0.164_{(106)}$	
	0.148		$0.149_{(123)}$		$0.149_{(220)}$	$0.147_{(242)}$	$0.147_{(113)}$	
730	0.547					$0.558_{(110)}$		
	0.410			$0.411_{(100)}$				
	0.320					$0.327_{(020)}$		
	0.277						$0.273_{(100)}$	
	0.254		$0.256_{(320)}$				$0.250_{(012)}$	
	0.220			$0.218_{(013)}$	$0.258_{(200)}$	$0.211_{(313)}$	$0.227_{(013)}$	
	0.204	$0.203_{(100)}$					$0.204_{(014)}$	$0.203_{(211)}$
	0.183			$0.181_{(202)}$				
	0.158		$0.158_{(103)}$		$0.185_{(212)}$	$0.158_{(042)}$	$0.158_{(110)}$	
					$0.158_{(303)}$			
790	0.250		$0.249_{(311)}$		$0.258_{(200)}$		$0.250_{(012)}$	
	0.222			$0.218_{(013)}$				
	0.204	$0.203_{(100)}$					$0.204_{(014)}$	$0.203_{(211)}$
	0.156		$0.156_{(103)}$		$0.158_{(303)}$	$0.156_{(042)}$	$0.156_{(110)}$	$0.155_{(120)}$

[a] The amorphous MoS_2 pattern may correspond to a Fe–Mo–S phase.

expected to result in an increase in the active area of the system as metal atoms are incorporated in the edge regions constituting the side of the pits. It is important to appreciate that all the events described above will be occurring simultaneously so that, at any given time, a variety of particle morphologies are present, which are constantly un-

TABLE 4

Calculated Values of H_2S/H_2 in the Environmental Cell of the CAEM

Temperature °C	H_2S/H_2 ratio		
	Co/MoS_2	Ni/MoS_2	Fe/MoS_2
200	1.5×10^{-7}	2.3×10^{-7}	1.5×10^{-7}
300	4.2×10^{-6}	5.7×10^{-6}	9.0×10^{-6}
400	4.4×10^{-5}	5.5×10^{-5}	1.7×10^{-5}
500	2.7×10^{-4}	3.0×10^{-4}	1.5×10^{-4}
600	1.0×10^{-3}	1.1×10^{-3}	8.2×10^{-3}
700	3.3×10^{-3}	3.3×10^{-3}	3.2×10^{-3}
800	8.1×10^{-3}	8.0×10^{-3}	9.7×10^{-3}

dergoing change from hemispherical to flat structures and vice versa. Such changes are controlled by the chemical nature of the underlying support.

The catalyzed reduction of molybdenum disulfide by these metals can be contrasted with that in the absence of additives, where attack appeared to be restricted to edges and steps. Moreover, the onset of this process did not occur until 675°C and the rate of reaction did not reach a measurable level until the temperature was raised to 725°C (*5*). It was suggested that since pits were not formed in the uncatalyzed reaction, this observation pointed to the fact that hydrogen discriminated in its chemisorption behavior, attacking only the edge sites. This claim was supported by earlier surface science studies which demonstrated that hydrogen was incapable of removing sulfur atoms from the basal plane of a sulfide surface which contained a significant number of defect sites (*6*).

The agreement between the apparent activation energies obtained for the hydrogenation of molybdenum disulfide in the presence of iron, cobalt, and nickel from the controlled atmosphere electron microscopy (edge recession and pit expansion) and macroscale experiments performed in the microbalance is excellent. This indicates that the rate-controlling step is the same and that any other factors affecting the overall value are also operative in both cases. Although we cannot state with any degree of certainty what the precise nature of the rate-determining step is in these systems, one can speculate that since the major function of the metal catalyst is to promote the removal of sulfur atoms from both edge and basal plane regions to form H_2S, then rupture of Mo–S bonds is a critical step in the process. The

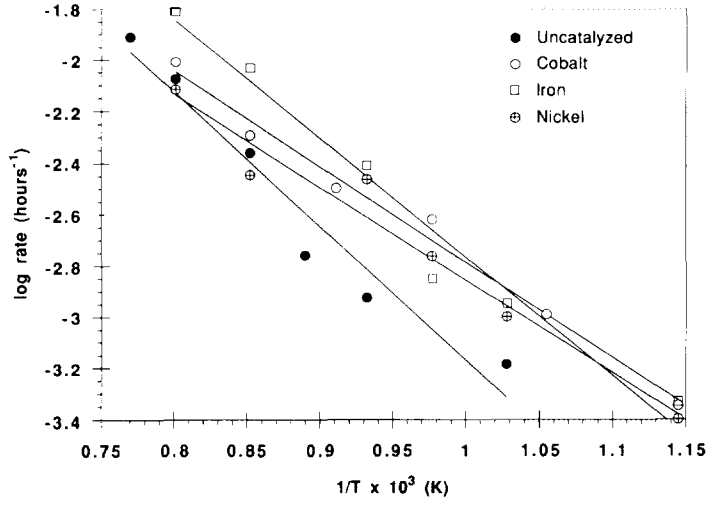

FIG. 7. Arrhenius plots of bulk kinetic data of the reduction of molybdenum disulfide in the absence of any additive and in the presence of ferromagnetic metals.

essential difference between the uncatalyzed and catalyzed reactions may lie in the ability of the ferromagnetic metal particles to provide an extra source of hydrogen atoms which are responsible for not only removing sulfur from edge regions but also initiating attack on the basal planes and in this context it would appear that iron-based particles perform this function more readily than the two other catalysts.

It is interesting to compare the results obtained from direct observation of the reactions with those obtained by other workers using a variety of techniques. Tanaka and Okuhara (*2*) used a deuterium tracer method to elucidate the reaction mechanism and crystallographic orientation of active sites for the reactions taking place on molybdenum disulfide single crystals. They found that hydrogenation and isomerization reactions of olefins occurred at the edge regions, but the active sites for the two reactions were entirely different in their catalytic action. Such differences in catalytic ability of these sites exposed at the edge regions may be caused by the different degrees of coordinated unsaturation.

Richardson (*19*) suggested that the following reactions occurred when hydrogen adsorbed on unpromoted molybdenum disulfide during the activation stage.

$$H_2 + S^{2-} = (H_2S)_{ads} + 2e^-$$

$$(H_2S)_{ads} = (H_2S).$$

S^{2-} ions are removed from the lattice which leads to the generation of sulfur vacancies. Based on this study and other work it may be concluded that hydrogen adsorbs on molybdenum disulfide crystals and eventually reacts to form hydrogen sulfide; however, the rate of this reaction is very slow unless catalysts are present.

Topsøe and co-workers (*20*) suggested that the mechanism for the hydrodesulfurization reaction requires an anion vacancy. In molybdenum disulfide, such an anion vacancy could be created according to the reaction,

$$2Mo^{4+} + S^{2-} + H_2 \longrightarrow 2Mo^{3+}\square + H_2S, \qquad \square \text{ anion vacancy.}$$

Promoters, particularly ferromagnetic metals, might be expected to enhance the number of such vacancies and thereby increase the catalytic activity of the structure.

Continuous observation of the events occurring at edge regions of the sulfide crystals indicated that as the temperature was progressively raised needle-like structures were formed and increased in size at the expense of material in the substrate. This phenomenon can be rationalized according to the notion that a new phase is being formed, such as an alloy consisting of molybdenum and the ferromagnetic metal or a sesquisulfide, Mo_2S_3. An appreciation of the complexity of the chemistry occurring during these reactions is gained from the information derived from the *in situ* electron diffraction studies and in order to understand the subtle differences exhibited by the three metals it is necessary to consider each system separately. In all cases, however, the appearance of the Mo_2S_3 phase in the electron diffraction patterns can be used as a fingerprint to indicate the onset of the catalytic reduction process.

$Co/MoS_2 - H_2$

From examination of the phase equlibria data (*21*) it is apparent that bulk cobalt sulfides will only be thermodynamically stable at the highest temperatures used in these experiments. At temperatures below 655°C the data indicate that cobalt is present primarily in the fully reduced state, either as the free metal or combined with molybdenum. It should be borne in mind, however, that since electron diffraction is a bulk technique a cobalt particle encapsulated with a monolayer of sulfur would give the pattern corresponding to the metallic state. In such circumstances selected chemical probe reactions, sensitive to the nature of the catalyst particle surface, will provide a more accurate assessment of the chemical nature of the reactive surface. In this context it

is interesting to draw attention to previous studies conducted in this laboratory (*22*) which demonstrated that when cobalt particles supported on molybdenum disulfide were initially treated in hydrogen at 500°C they completely lost their ability to catalyze the decomposition of acetylene leading to the growth of a filamentous carbon deposit. It was suggested that poisoning of the cobalt activity was due to the accumulation of a monolayer of sulfur on the metal particle surfaces. Based on these experiments it is therefore probable that in the present system both cobalt and cobalt–molybdenum alloy particles are covered by a monolayer of sulfur.

Among the many models proposed for the structure of the cobalt-promoted molybdenum disulfide HDS catalysts (*23*), recent work indicates that Co atoms are incorporated into Mo vacancies at the edge locations of the MoS_2 microcrystals (*7*, *24*, *25*). It has been reported that X-ray diffraction results of the proposed active-phase, "CoMoS" are identical to those of polycrystalline MoS_2 (*20*). In the present study, we have used single crystal molybdenum disulfide and the appearance of an amorphous phase might suggest that in the presence of a metal additive break up into smaller fragments occurs. In contrast, when the reduction was performed in the absence of a catalyst this transformation was not observed (*5*). Alternatively, one might speculate that these rings are attributable to the existence of a CoMoS phase; however, such a conclusion must be regarded as extremely tentative in nature.

Ni/MoS₂ – H₂

In this system the formation of a bulk sulfide, Ni_3S_2, is thermodynamically favored at low temperatures (*21*) and from the *in situ* electron diffraction results presented here its presence is detected at a temperature of 300°C and the appearance of another metal sulfide phase, NiS, is indicated at about 500°C. The formation of the sulfide Ni_3S_2 has been identified by EXAFS studies performed on carbon-supported sulfided nickel and sulfided nickel–molybdenum bimetallic catalysts under similar conditions (*26*). The electron diffraction analysis also indicates that a fraction of the deposited nickel remains in the fully reduced bulk state; however, we believe that these particles and also those containing a mixture of nickel and molybdenum will have a layer of surface sulfur atoms. A "NiMoS" structure has been reported in which the nickel atoms are incorporated into vacancies in the Mo plane of MoS_2 crystallites (*27*). If such a phase is formed in the current experiments it might conceivably appear as polycrystalline MoS_2 in the diffraction patterns.

Fe/MoS₂ – H₂

Electron diffraction analysis of these specimens shows that a fraction of the iron readily undergoes interaction with MoS_2 to form a stable bulk sulfide, FeS, at temperatures as low as 225°C and this finding is consistent with the predictions of bulk thermodynamics data (*21*). On increasing the temperature, we see that there is a tendency for iron to react with molybdenum generated during the reduction reaction to form a combination of a bimetallic and mixed metal sulfide compounds. It is significant that with this additive no evidence for the existence of fully reduced bulk iron was found in the temperature range 225 to 665°C and did not appear until specimens were heated up to 730°C. Finally, by analogy with the previous systems it is possible that the rings which have been assigned to polycrystalline MoS_2 can be attributed to the formation of a "FeMoS" phase (*28*, *29*).

In summary, the controlled atmosphere electron microscopy studies combined with *in situ* electron diffraction analysis have demonstrated that in all these reactions a variety of metal sulfides and intermetallic compounds, whose existence depends on a number of factors can be formed. These included the location of the ferromagnetic metal and its interaction with the molybdenum disulfide support and the temperature

at which the system is heated in hydrogen. It is therefore not unreasonable to expect that such compounds will exhibit wide differences in their catalytic activity.

APPENDIX

H_2S/H_2 Values in the Environmental Cell of the CAEM

The data of reaction rate as a function of temperature (Fig. 7) were used to determine the rates of H_2S production and then compute the H_2S/H_2 ratio existing in the environmental cell of the CAEM, during studies where the catalytic reduction of MoS_2 was used as a source of sulfur. The transmission specimens of MoS_2 are exposed to an amount of H_2S in the gas phase governed by the rate of reduction of the solid sulfide. Based on the typical dimensions of the MoS_2 crystals used in electron microscopy experiments (~1.5 mm in diameter and 75 nm thick), a metal loading of 10% Co/MoS_2, 12% Ni/MoS_2, and 17% Fe/MoS_2 by weight was estimated. Using this information the rates of H_2S production at selected temperatures were determined from the thermogravimetric experiments.

With an operating cell pressure of 2.0 Torr air and microscope column pressure of 1×10^{-6} Torr, the flow rate of 0.55 ml/min was measured through two 70-μm apertures in the environmental cell. An estimate of the H_2 flow rate through the cell at an operating pressure of 0.2 Torr has been made using the basic orifice equation, which states that flow through an orifice is proportional to the square root of the pressure difference.

$$u_o = [C_o/(1 - \beta^4)^{1/2}] \cdot [2g_c(P_a - P_b)/\rho]^{1/2},$$

where u_o = velocity through the orifice, P_a = pressure within the gas cell, P_b = pressure in the microscope column, C_o = orifice coefficient, β = ratio of orifice diameter to pipe diameter, g_c = gravitational constant, ρ = density.

From these calculations the estimated flow rate is 0.1 ml/min at 0.2 Torr H_2. At elevated temperatures this flow rate will tend to increase slightly due to decrease density and viscosity of the gases in the cell. When this information is combined with the experimentally determined H_2S production rates and the ratio H_2S/H_2 created in the environmental cell from the catalytic reduction of MoS_2 under various conditions, the values listed in Table 4 were obtained.

ACKNOWLEDGMENT

Financial support for this work was provided by the Department of Energy, Basic Energy Sciences, Grant DE-FG05-89ER14076.

REFERENCES

1. Tsigdinos, G. A., *in* "Topics in Current Chemistry," Vol. 76, p. 65. Springer-Verlag, New York, 1978.
2. Tanaka, K., and Okuhara, T., *J. Catal.* **78,** 155 (1982).
3. Bahl, O. P., Evans, E. L., and Thomas, J. M., *Proc. R. Soc. A* **306,** 53 (1968).
4. Chianelli, R. R., Ruppert, A. F., Behal, S. K., Kear, B. H., Wold, A., and Kershaw, R., *J. Catal.* **92,** 56 (1985).
5. Baker, R. T. K., Chludzinski, J. J., and Sherwood, R. D., *J. Mat. Sci.* **22,** 3831 (1987).
6. Farias, M. H., Gellman, A. J., Somorjai, G. A., Chianelli, R. R., and Liang, K. S., *Surf. Sci.* **140,** 181 (1984).
7. Sorensen, O., Clausen, B. S., Candia, R., and Topsøe, H., *Appl. Catal.* **13,** 363 (1985).
8. Kamaratos, M., and Papageorgapolus, C. A., *Surf. Sci.***160,** 451 (1985).
9. Papageorgapolus, C. A., and Kamaratos, M., *Surf. Sci.* **164,** 353 (1985).
10. Yogjun, H., and Zhangda, L., *Surf. Sci.* **192,** 283 (1987).
11. Baker, R. T. K., and Harris, P. S., *J. Phys. E.* **5,** 792 (1972).
12. Hennig, G., *in* "Chemistry and Physics of Carbon" (P. L. Walker, Jr., Ed.), Vol. 2, p. 1. Dekker, New York, 1966.
13. Rodriguez, N. M., Oh, S. G., Downs, W. B., Pattabiraman, P., Baker, R. T. K., *Rev. Sci. Inst.* **61,** 1863 (1990).
14. Dudnik, E. M., and Oganesyan, V. K., *Poroshk. Metall.* **6,** 60 (1966).
15. Pearson, W., *in* "Handbook of Lattice Spacings and Structures of Metals and Alloys" (P. Villars and L. D. Calvert Eds.). American Society for Metals, Metals Parik, OH, 1967.
16. Cox, E., *in* "Crystal Data, Determinative Tables" (J. Donnay, Ed.). American Crystallographic Association, 1963).
17. Taylor, A., and Kagle, B., "Crystallographic Data on Metal and Alloy Structures." Dover, New York, 1963.

18. Smithells, C. "Metals Reference Book." Butterworths, Washington, D.C., 1962.
19. Richardson, J. T., *J. Catal.* **112,** 313 (1988).
20. Topsøe, H., Clausen, B. S., Candia, R., Wivel, C., and Morup, S., *J. Catal.* **68,** 433 (1981).
21. McKinley, J. B., *in* "Catalysis" (P. Emmett, Ed.), Vol. V. Reinhold, New York, 1975.
22. Chen, C. C., Rodriguez, N. M., and Baker, R. T. K., *in* "Studies in Surface Science and Catalysis—Catalyst Deactivation 1991" (C. H. Bartholomew and J. J. Butt, Eds.), p. 169. Elsevier, Amsterdam, 1991.
23. Topsøe, H., and Clausen, B. S., *Catal. Rev. Sci. Eng.* **26,** 395 (1984).
24. Derouane, E. G., Pedersen, E., Clausen, B. S., Gabelica, Z., Candia R., and Topsøe H., *J. Catal.* **99,** 253 (1986).
25. Bowens, S. M. A. M., Prins, R., de Beer, V. H. J., and Koningsberger, D. C., *J. Phys. Chem.* **94,** 3711 (1990).
26. Louwers, S. P. A., and Prins, R., *J. Catal.* **133,** 94 (1992).
27. Topsøe, N-Y, and Topsøe, H., *J. Catal.* **84,** 386 (1983).
28. Topsøe, H., Clausen, B. S., Candia, R., Wivel, C., and Morup, S., *Bull. Soc. Chim. Belg.* **90,** 1189 (1984).
29. Ramselear, W. L. T. M., Craje, M. W. J., Gerkema, E., de Beer, V. H. J., and van de Kraan, A. M., *Appl. Catal.* **54,** 217 (1989).